International Journal of Structural Stability and Dynamics

Optimal design of inertial amplifier base isolators for dynamic response control of multi-storey buildings

Sudip Chowdhury*
Civil Engineering Department, Indian Institute of Technology Delhi, India
sudip.chowdhury@civil.iitd.ac.in

Arnab Banerjee
Civil Engineering Department, Indian Institute of Technology Delhi, India
abanerjee@iitd.ac.in

Sondipon Adhikari
James Watt School of Engineering, The University of Glasgow, Glasgow, UK
Sondipon.Adhikari@glasgow.ac.uk

Received (Day Month Year)
Accepted (Day Month Year)

The optimal design of inertial amplifier base isolators (IABI) for dynamic response mitigation of multi-storey buildings subjected to base excitations has been studied in this paper. In order to achieve the closed-form expressions for optimal design parameters of IABI, H_2 optimization method has been employed. The effectiveness of the closed-form expressions for optimal design parameters was evaluated by determining the isolated structures' frequency and time domain responses and comparing them to the corresponding responses obtained from equivalent uncontrolled structures. A numerical study employing the Newmark-beta method is conducted to obtain time-domain responses using near-field earthquake base excitation. The response reduction capacity (%) of the optimum inertial amplifier base isolator is compared to the response reduction capacity (%) of the optimum traditional base isolators, demonstrating that inertial amplifiers have increased the vibration reduction performance of traditional base isolators by 50 to 60 %. All the outcomes from the study are mathematically accurate and also feasible for practical design purposes.

Keywords: Inertial amplifier base isolator;H_2 optimization method; Traditional base isolator; Harmonic and white-noise random; Near-field earthquake base excitation.

1. Introduction

The base isolation devices are significantly preferable among all passive vibration control devices for protecting the structures and human lives from natural calamities like seismic events [1,2,3,4,5,6,7]. The vibration isolation devices are installed in many structures such as aerospace [8], vehicle suspension [9], liquid storage tanks [10],

*Corresponding author: Sudip Chowdhury, Email id: sudip.chowdhury@civil.iitd.ac.in

buildings [11,12,13,14], bridges [15,16], aircraft landing gear [17,18] for mitigating the dynamic responses during vibration. For building structures, the base isolation devices are installed between the foundation and superstructure [19,20]. Along with the linear traditional base isolators (TBI), the nonlinear traditional isolators [21,22,23] are also very much preferable in industry such as new zealand bearing [24], lead rubber bearing [25], resilient friction base isolator [26], friction-pendulum system [27,28], pure-friction system [29]. Simplified but functional comprehension can be developed from the analytical solution of a linear traditional base isolator (TBI) consisting of single degrees of freedom system with springs, masses and viscous dampers. The nonlinear traditional isolators have been designed by altering the viscous dampers of the linear system with hysteresis damping. To achieve the robust performance from the base isolators, the governing parameters must be optimized. H_2 and H_∞ optimization methods [30,31,32,33] are very much useful to derive closed-form expressions for optimal design parameters for vibration isolation devices [34,35,36]. Hence, these optimizations methods are adopted and implemented in this paper. H_2 optimization method is a stochastic process and the optimal closed-form expressions are deriving from the standard deviation of primary structure's responses when the isolated structures are subjected to random vibration [37].

Recently, researchers are applying effective mass amplification devices to enhance the response reduction capacity of traditional base isolation devices, which are capable of reducing the dynamic responses of low-frequency contained structures [38,39,40]. Inertial amplifiers are one of the mass amplification devices which can provide large wide-bandgaps at low frequencies [41,42,43,44,45]. These mass amplification devices are applied in traditional base isolation devices for enhancing their vibration reduction capacity; however, most of the research conducted for structural members, single-storey buildings, and single degree of freedom systems the conceptualized version of a bridge, water tank, building or tower [46,47,48,49]. The applications of inertial amplifiers to traditional base isolators for multi-storey buildings or multi-degree-of-freedom systems are not presented in state of the art.

To address the above-mentioned research gap from state of the art, the optimal design of inertial amplifier base isolators (IABI) for vibration mitigation of multi-storey buildings subjected to base excitations has been studied in this paper. Moreover, the closed-form expressions for optimal design parameters of IABI have been derived using H_2 optimization methods which are one of the main contributions of the paper. The vibration reduction capacity of optimum IABI has been compared with the vibration reduction capacity of optimum traditional base isolator (TBI).

2. Methodology

2.1. *Structural Model*

The inertial amplifier base isolators are installed at the base of the multi-storey buildings subjected to base excitations. The isolated multi-storey buildings are mathematically conceptualized as multi-degree-of-freedom systems (MDOF) having spring-mass with dash-pot to determine dynamic responses. Hence, the mathematical diagram has been drawn and displayed in Figure 1 (a). Subsequently, the schematic diagram of an inertial amplifier and corresponding free-body diagrams has been shown in Figure 1 (b) and (c), where points 1 and 2 are indicated as two terminals. 'N' defines the number of floors for the superstructure. m_N, k_N, and c_N define the mass, stiffness, and damping of the top floor. m_b, k_b, and c_b define

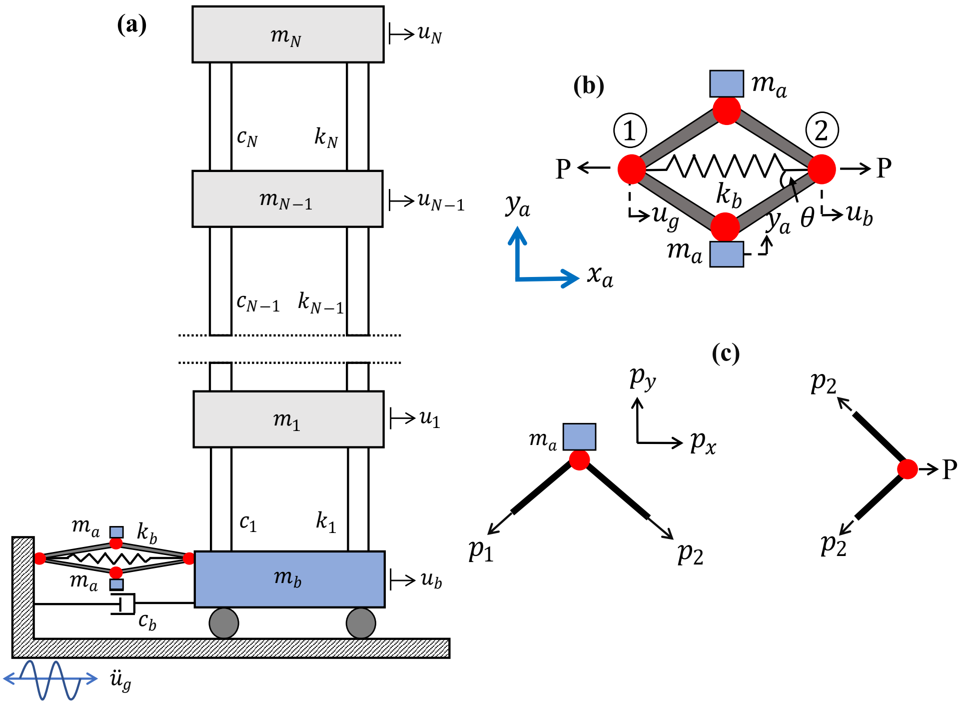

Figure 1. (a) A multi-storey building isolated by inertial amplifier base isolator subjected to base excitation $\ddot{u}_g$. (b) The schematic diagram of inertial amplifier base isolator. (c) Free-body diagram.

the mass, stiffness, and damping of the IABI without considering the mass amplification effect of inertial amplifiers. However, those are converted to m_{ia}, k_{ia}, and c_{ia} after considering the mass amplification effect of inertial amplifiers, define as effective mass, stiffness, and damping. m_a define the top and bottom masses of the inertial amplifiers.

2.2. *Equations of motion*

The derivation of effective mass must be derived before determining the equations of motion for complete isolated structure. Therefore, x_a and y_a are considered the displacement response of the vertical and bottom masses m_a in x and y-directions which have derived as

$$x_a = \frac{u_b + u_g}{2} \quad \text{and} \quad y_a = \pm \frac{u_b - u_g}{2\tan\theta} \tag{2.1}$$

The inertial forces developed through masses m_a are derived as

$$p_x = m_a \ddot{x}_a \quad \text{and} \quad p_y = m_a \ddot{y}_a \tag{2.2}$$

where p_x and p_y refer the inertial forces which have been generated in x and y-directions. The forces generated through the rigid links are denoted as p_1 and p_2. Hence, the exact closed-form expressions for p_1 and p_2 have been derived as

$$p_1 = \frac{1}{2}\left(\frac{p_y}{\sin\theta} - \frac{p_x}{\cos\theta}\right) \quad \text{and} \quad p_2 = \frac{1}{2}\left(\frac{p_y}{\sin\theta} + \frac{p_x}{\cos\theta}\right) \tag{2.3}$$

Using Eq. (2.3), the closed-form expression for total reaction force has been derived as

$$\begin{aligned} P &= 2p_2\cos\theta + k_b(u_b - u_g) \\ &= \underbrace{\frac{0.5m_a}{\tan^2\theta}}_{d_1}(\ddot{u}_b - \ddot{u}_g) + \underbrace{0.5m_a}_{d_2}(\ddot{u}_b + \ddot{u}_g) + k_{ia}(u_b - u_g) \end{aligned} \tag{2.4}$$

where $d_1 = \left(0.5m_a/\tan^2\theta\right)$ and $d_2 = 0.5m_a$ are the effective mass values which have been added with the base mass m_b. Hence, The total effective mass for the inertial amplifier base isolators have been derived as

$$m_{ia} = m_b + 0.5m_a\left(1 + \frac{1}{\tan^2\theta}\right) \tag{2.5}$$

Simultaneously, using Eq. (2.5), the total effective stiffness for the inertial amplifier base isolators have been derived as

$$k_{ia} = m_{ia}\omega_b^2 \tag{2.6}$$

The total effective damping for inertial amplifier base isolator has been derived as

$$c_{ia} = 2\zeta_b m_{ia}\omega_b \tag{2.7}$$

Total static mass of IABI has been derived as $m_T = m_b + 2m_a$. Before determining the dynamic responses of structure isolated by IABI, the mass amplification effect of IABI needs to be determined. Hence, the ratio of amplifier mass to the total static mass of the isolator has been determined as

$$\alpha = \frac{m_a}{m_T} \quad \text{and} \quad m_a = \left(\frac{\alpha}{1 - 2\alpha}\right)m_b \tag{2.8}$$

The ratio of base mass to the total static mass of the isolator has been determined as

$$\beta = \frac{m_b}{m_T} = (1 - 2\alpha) \tag{2.9}$$

The effective mass amplifications of IABI have been determined by dividing the effective mass by the total static mass of the isolator. Therefore, the mathematical expression for effective mass amplifications m_f has been derived as

$$m_f = \frac{m_{ia}}{m_T} = (1 - 2\alpha) + 0.5\alpha\left(1 + \frac{1}{\tan^2\theta}\right) \tag{2.10}$$

The change of effective stiffness with respect to the total static stiffness needs to be investigated. Hence, the ratio of effective stiffness to the static stiffness of the isolator k_f has been determined as

$$k_f = \frac{k_{ia}}{k_b} = 0.5\left(1 + \frac{1}{\tan^2\theta}\right)\left(\frac{\mu_a}{\mu_b}\right) + 1 \tag{2.11}$$

μ_a and μ_b define the ratio of amplifier mass and base mass to the main structural mass of the isolated structure. The effect of the inertial amplifier on the static mass of the IABI has been investigated thoroughly. Hence, the contour plot of Equation 2.10 as a function of the ratio of amplifier mass to the total static mass of isolator and inertial angle has been displayed in Figure 2 (a). The result shows that

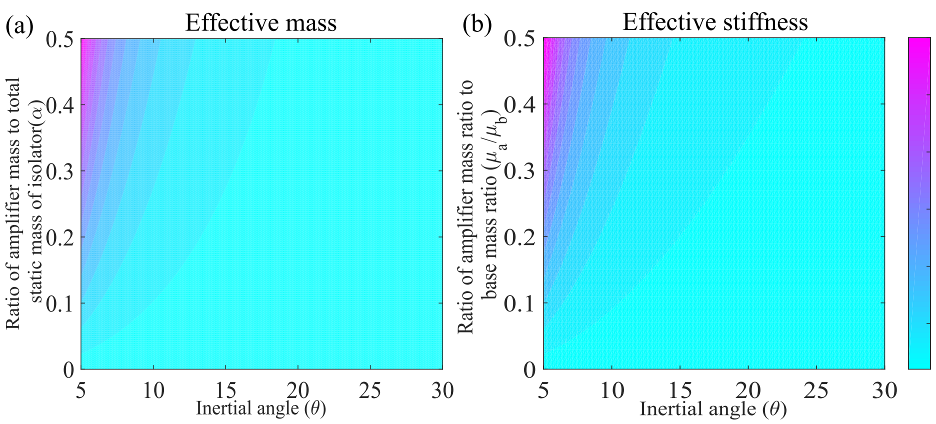

Figure 2. (a) The contour plot of effective mass as a function of ratio of amplifier mass to total static mass of isolator and inertial angle, (b) The contour plot of effective stiffness as a function of ratio of amplifier mass ratio to base mass ratio of isolator and inertial angle.

the effective mass amplification occurred at $\theta \leq 30^o$, which have been identified as the critical angles for the IABI. Apart from that, a significant mass amplification occurred at $5^o \leq \theta \leq 14^o$. Therefore, $\theta = 14^o$ has been applied throughout the paper to determine the dynamic responses and corresponding response reduction capacity. Overall, the lower inertial angles provide superior vibration attenuation properties than the higher inertial angle for IABI. A significant amount of effective mass amplifications have also occurred for higher values of the amplifier mass ratio to the isolator's total static mass. Therefore, lower inertial angle and higher values of the ratio of amplifier mass to the total static mass of the isolator have been recommended to achieve robust vibration attenuation performance of IABI. The effect of the inertial amplifier on the static stiffness of the IABI has also been investigated. Hence, the contour plot of Equation 2.11 as a function of the ratio of amplifier mass ratio to base mass ratio of isolator and inertial angle has been displayed in Figure 2 (b). The effective stiffness ratio to the isolator's static stiffness has been significantly increased for $5^o \leq \theta \leq 14^o$. A significant amount of the effective stiffness ratio to the isolator amplifications' static stiffness has also occurred for higher values of the ratio amplifier mass ratio to base mass ratio. Hence, lower inertial angle and higher values of the effective stiffness ratio to the isolator's static stiffness have been recommended to achieve robust vibration attenuation performance for IABI. The equations of motion of IABI for multi-storey buildings are derived as

$$\begin{aligned}[\mathbf{M}_s]\{\ddot{\mathbf{x}}_s\} + [\mathbf{C}_s]\{\dot{\mathbf{x}}_s\} + [\mathbf{K}_s]\{\mathbf{x}_s\} &= -[\mathbf{M}_s]\{\mathbf{r}\}(\ddot{u}_g + \ddot{x}_b)\\ m_{ia}\ddot{x}_b + c_{ia}\dot{x}_b + k_{ia}x_b - k_1x_1 - c_1\dot{x}_1 &= -m_{ia}\ddot{u}_g\end{aligned} \tag{2.12}$$

where, $x_b = u_b - u_g$, defines the relative displacement of IABI w.r.t the displacement of the base excitation. $x_N = u_N - u_b$, $x_{N-1} = u_{N-1} - u_b$. $x_1 = u_1 - u_b$ define as the relative displacement of each floor w.r.t the displacement of IABI. $[\mathbf{M}_s]$, $[\mathbf{C}_s]$, and $[\mathbf{K}_s]$ define the mass, damping, and stiffness matrices of the superstructure. $\{\mathbf{x}_s\} = \{x_1, x_2, x_3, \cdots, x_N\}$, $\{\ddot{\mathbf{x}}_s\}$, and $\{\dot{\mathbf{x}}_s\}$ are the main structure's undetermined displacement, acceleration, and velocity vectors. The influence coefficient vector for loading function considers as $\{\mathbf{r}\} = \{1, 1, 1, \cdots, 1\}$. Initially, the mathematical model of five-storey building is considered to derive the closed-form expressions for optimal design parameters of IABI analytically. The equations of motion for isolated five-storey building are derived as

$$\begin{aligned}
&m_{ia}\ddot{x}_b + c_{ia}\dot{x}_b + k_{ia}x_b - k_1x_1 - c_1\dot{x}_1 = -m_{ia}\ddot{u}_g\\
&m_1\ddot{x}_1 + (c_1 + c_2)\dot{x}_1 - c_2\dot{x}_2 + (k_1 + k_2)x_1 - k_2x_2 + m_1\ddot{x}_b = -m_1\ddot{u}_g\\
&m_2\ddot{x}_2 - c_2\dot{x}_1 + (c_2 + c_3)\dot{x}_2 - c_3\dot{x}_3 - k_2x_1 + (k_2 + k_3)x_2 - k_3x_3 + m_2\ddot{x}_b = -m_2\ddot{u}_g\\
&m_3\ddot{x}_3 - c_3\dot{x}_2 + (c_3 + c_4)\dot{x}_3 - c_4\dot{x}_4 - k_3x_2 + (k_3 + k_4)x_3 - k_4x_4 + m_3\ddot{x}_b = -m_3\ddot{u}_g\\
&m_4\ddot{x}_4 - c_4\dot{x}_3 + (c_4 + c_5)\dot{x}_4 - c_5\dot{x}_5 - k_4x_3 + (k_4 + k_5)x_4 - k_5x_5 + m_4\ddot{x}_b = -m_4\ddot{u}_g\\
&m_5\ddot{x}_5 - c_5\dot{x}_4 + c_5\dot{x}_5 - k_5x_4 + k_5x_5 + m_5\ddot{x}_b = -m_5\ddot{u}_g
\end{aligned} \tag{2.13}$$

where m_1, m_2, m_3, m_4, m_5 define the masses of each floor that have been considered as identical and represented as m_s (i.e., $m_1 = m_2 = m_3 = m_4 = m_5 = m_s$). k_1, k_2, k_3, k_4, k_5 define the stiffness of each floor that have been considered as identical and represented as k_s (i.e., $k1 = k_2 = k_3 = k_4 = k_5 = k_s$). c_1, c_2, c_3, c_4, c_5 define the viscous damping of each floor that have been considered as identical and represented as c_s (i.e., $c1 = c_2 = c_3 = c_4 = c_5 = c_s$). Now considered that the isolated structure is subjected to harmonic excitation. Therefore, the steady-state solutions for the displacement responses of the isolated multi-storey building have been considered as $x_1 = X_1 e^{\mathrm{i}\omega t}$, $x_2 = X_2 e^{\mathrm{i}\omega t}$, $x_3 = X_3 e^{\mathrm{i}\omega t}$, $x_4 = X_4 e^{\mathrm{i}\omega t}$, $x_5 = X_5 e^{\mathrm{i}\omega t}$, $x_b = X_b e^{\mathrm{i}\omega t}$, and $\ddot{u}_g = U_g e^{\mathrm{i}\omega t}$. After substituting the steady-state solutions into Eq. (2.13), the transfer function has been derived as

$$\begin{bmatrix} A_1 & A_2 & 0 & 0 & 0 & q^2 \\ A_2 & A_1 & A_2 & 0 & 0 & q^2 \\ 0 & A_2 & A_1 & A_2 & 0 & q^2 \\ 0 & 0 & A_2 & A_1 & A_2 & q^2 \\ 0 & 0 & 0 & A_2 & A_3 & q^2 \\ A_2 & 0 & 0 & 0 & 0 & A_4 \end{bmatrix} \begin{Bmatrix} X_1 \\ X_2 \\ X_3 \\ X_4 \\ X_5 \\ X_b \end{Bmatrix} = - \begin{bmatrix} 1 \\ 1 \\ 1 \\ 1 \\ 1 \\ \mu_{ia} \end{bmatrix} U_g \tag{2.14}$$

$$\begin{aligned} & q = \mathrm{i}\omega, A_1 = 4\,\zeta_s q\omega_s + q^2 + 2\,{\omega_s}^2, A_2 = -2\,\zeta_s q\omega_s - {\omega_s}^2, \\ & A_3 = 2\,\zeta_s q\omega_s + q^2 + {\omega_s}^2 \quad \text{and} \quad A_4 = 2\,q\omega_b\zeta_b\mu_{ia} + q^2\mu_{ia} + \mu_{ia}{\omega_b}^2 \end{aligned} \tag{2.15}$$

where $\mu_b = m_b/m_s$ defines as base mass ratio and $\mu_{ia} = m_{ia}/m_s$ defines as "effective base mass ratio". $\mu_a = m_a/m_s$ defines as "amplifiers mass ratio". $\eta_b = \omega_b/\omega_s$ defines as the frequency ratio of IABI. The frequency of each floor determines as $\omega_s = \sqrt{k_s/m_s}$. The viscous damping ratio of each floor considers as $\zeta_s = \frac{c_s}{2m_s\omega_s}$. The displacement response of top floor has been derived and expressed as

$$H_5(q) = \frac{\begin{pmatrix} -2\,q^9\zeta_b\mu_{ia}\omega_b - 18\,q^7\zeta_b\mu_{ia}\omega_b{\omega_s}^2 - 56\,q^5\zeta_b\mu_{ia}\omega_b{\omega_s}^4 \\ -70\,q^3\zeta_b\mu_{ia}\omega_b{\omega_s}^6 - 30\,q\zeta_b\mu_{ia}\omega_b{\omega_s}^8 - q^8\mu_{ia}{\omega_b}^2 \\ -9\,q^6\mu_{ia}{\omega_b}^2{\omega_s}^2 - 28\,q^4\mu_{ia}{\omega_b}^2{\omega_s}^4 - 35\,q^2\mu_{ia}{\omega_b}^2{\omega_s}^6 \\ -15\,\mu_{ia}{\omega_b}^2{\omega_s}^8 \end{pmatrix}}{\Delta_b} \tag{2.16}$$

The values of structural damping considers as 0 (i.e., $\zeta_s = 0$) to reduce the length of the closed-form expressions for controlled structural responses. This consideration will helps to derive the closed-form expressions for optimal design parameters. Now, the displacement response of IABI has been derived as

$$H_b(q) = \frac{\begin{pmatrix} -q^{10}\mu_{ia} - 9\,q^8\mu_{ia}{\omega_s}^2 - 28\,q^6\mu_{ia}{\omega_s}^4 - 35\,q^4\mu_{ia}{\omega_s}^6 \\ -15\,q^2\mu_{ia}{\omega_s}^8 - \mu_{ia}{\omega_s}^{10} - q^8{\omega_s}^2 - 8\,q^6{\omega_s}^4 \\ -21\,q^4{\omega_s}^6 - 20\,q^2{\omega_s}^8 - 5\,{\omega_s}^{10} \end{pmatrix}}{\Delta_b} \tag{2.17}$$

The closed-form expression for Δ_b has been derived as

$$\Delta_b = \left(\begin{array}{c} q^{12}\mu_{ia} + 2\,q^{11}\zeta_b\mu_{ia}\omega_b + \left({\omega_b}^2\mu_{ia} + 9\,\mu_{ia}{\omega_s}^2 + {\omega_s}^2\right) q^{10} \\ +18\,q^9\zeta_b\mu_{ia}\omega_b{\omega_s}^2 + \left(9\,\mu_{ia}{\omega_b}^2{\omega_s}^2 + 28\,\mu_{ia}{\omega_s}^4 + 8\,{\omega_s}^4\right) q^8 \\ +56\,q^7\zeta_b\mu_{ia}\omega_b{\omega_s}^4 + \left(28\,\mu_{ia}{\omega_b}^2{\omega_s}^4 + 35\,\mu_{ia}{\omega_s}^6 + 21\,{\omega_s}^6\right) q^6 \\ +70\,q^5\zeta_b\mu_{ia}\omega_b{\omega_s}^6 + \left(35\,\mu_{ia}{\omega_b}^2{\omega_s}^6 + 15\,\mu_{ia}{\omega_s}^8 + 20\,{\omega_s}^8\right) q^4 \\ +30\,q^3\zeta_b\mu_{ia}\omega_b{\omega_s}^8 + \left(15\,\mu_{ia}{\omega_b}^2{\omega_s}^8 + \mu_{ia}{\omega_s}^{10} + 5\,{\omega_s}^{10}\right) q^2 \\ +2\,q\zeta_b\mu_{ia}\omega_b{\omega_s}^{10} + \mu_{ia}{\omega_b}^2{\omega_s}^{10} \end{array} \right) \tag{2.18}$$

2.3. H_2 optimization for white-noise random excitation

H_2 optimization has been performed to minimize the total energy of the isolated multi-storey building over all frequencies. It has been applied for this paper to derive the analytical closed-form expressions for optimal design parameters of IABI for vibration mitigation of multi-storey buildings, respectively [49,31]. The formulation for obtaining standard deviation of responses for multi-storey buildings isolated by IABI has been derived and presented in Appendix A. Hence, Eq. (2.18) is a 12^{th} order polynomial equation and the standard deviation of displacement of the top floor of the main structure has been derived as

$$\sigma_{x_5}^2 = \frac{S_0\pi\,\omega_b\left(220\,{\zeta_b}^2\mu_{ia}{\omega_s}^2 + 671\,\mu_{ia}{\omega_b}^2 + 225\,{\omega_s}^2\right)}{2{\omega_s}^6\zeta_b} \tag{2.19}$$

The optimal design parameters of IABI for a five-storey building have been derived using the formula listed below.

$$\frac{\partial\sigma_{x_5}^2}{\partial\zeta_b} = 0 \quad \text{and} \quad \frac{\partial\sigma_{x_5}^2}{\partial\omega_b} = 0 \tag{2.20}$$

Inserting $\sigma_{x_5}^2$ in the first equation of Eq. (2.20), the closed-form expression for damping ratio of IABI ζ_b has been derived and expressed as

$$\zeta_b = \frac{\sqrt{55}\sqrt{\mu_{ia}\left(671\,\mu_{ia}{\omega_b}^2 + 225\,{\omega_s}^2\right)}}{110\,\mu_{ia}\omega_s} \tag{2.21}$$

Equation (2.21) contains optimal frequency of IABI ω_b which needs to to be separated. To achieve that, Eq. (2.21) has been substituted in Eq. (2.22). Therefore, the modified standard deviation of displacement response has been derived as

$$\sigma_{x_5}^2 = \frac{S_0\pi\,\omega_b\left(1342\,\mu_{ia}{\omega_b}^2 + 450\,{\omega_s}^2\right)\sqrt{55}\mu_{ia}}{{\omega_s}^5\sqrt{\mu_{ia}\left(671\,\mu_{ia}{\omega_b}^2 + 225\,{\omega_s}^2\right)}} \tag{2.22}$$

Now, Eq. (2.22) has been substituted in second equation of Eq. (2.20) and the closed-form expression for optimal frequency of IABI ω_b has been derived as

$$(\omega_b)_{opt} = \frac{15\omega_s}{\sqrt{1342\,\mu_{ia}}} \quad \text{or} \quad (\omega_b)_{opt} = \frac{15\omega_s}{\sqrt{1342\,\left(\mu_b + 0.5\mu_a\left(1 + \frac{1}{\tan^2\theta}\right)\right)}} \tag{2.23}$$

The non-dimensional form of Eq. (2.23) has been derived below.

$$(\eta_b)_{opt} = \frac{15}{\sqrt{1342\,\left(\mu_b + 0.5\mu_a\left(1 + \frac{1}{\tan^2\theta}\right)\right)}} \tag{2.24}$$

Equation (2.23) has been substituted in Eq. (2.21) and Eq. (2.22) to derive the closed-form expression for optimal viscous damping ratio of IABI. Therefore, the optimal damping ratio of IABI has been derived as

$$(\zeta_b)_{opt} = \sqrt{\frac{45}{88\mu_{ia}}} \quad \text{or} \quad (\zeta_b)_{opt} = \sqrt{\frac{45}{88\left(\mu_b + 0.5\mu_a\left(1 + \frac{1}{\tan^2\theta}\right)\right)}} \tag{2.25}$$

3. Results and Discussion

3.1. *H_2 optimization*

The contour plot of Eq. (2.24) as a function of amplifier inertial angle (θ) and base mass ratio μ_b has been displayed in Figure 3 (a). The optimal frequency ratio of IABI has also decreased when the values of θ decreases. In fact, for $5^o < \theta < 14^o$ the values for frequency ratios are minimum. The primary goal of the research was to achieve robust vibration reduction capacity through a significant amount of effective mass amplifications. The least value for effective mass amplification in IABI has been observed at $\theta = 14^o$. Therefore, we want to investigate the vibration reduction performance of IABI at its lower mass amplification condition. The optimal frequency ratio of the inertial amplifier base isolator decreases when the base mass ratio increases. Same trend has also been observed for Figure 3 (b). However, the optimal frequency ratio of IABI increases when the inertial angle of the amplifier increases. $\theta = 14^o$ has been selected to plot Figure 3 (b). The contour plot of Eq. (2.24) as a function of amplifier mass ratio (μ_a) and base mass ratio μ_b has been displayed in Figure 3 (b). The optimal frequency ratio of IABI is decreased when the amplifier's mass ratio increases. Hence, higher base mass with higher amplifier's mass ratio of IABI has been recommended to design the optimal IABI for achieving the robust vibration reduction capacity. The variations of optimal damping ratio $(\zeta_b)_{opt}$ versus base mass ratio μ_b of IABI using Eq. (2.25) for different values of amplifier's mass ratio μ_a have been displayed Figure 4 (a). The optimal damping ratio of the inertial amplifier base isolator decreases when the base mass ratio increases. The optimal damping ratio of IABI is decreased when the amplifier's mass ratio increases. The variations of optimal damping ratio of IABI $(\zeta_b)_{opt}$ versus base mass ratio μ_b of IABI for different values of amplifier's inertial angle θ have been displayed Figure 4 (b). The optimal damping ratio of the inertial amplifier base isolator increases when the values of inertial angle increases. Overall, a higher base mass with lower amplifier's inertial angle (i.e.,$5^o < \theta < 14^o$) and amplifiers mass ratio has been recommended for designing the optimal IABI to achieve robust vibration reduction capacity. Overall, the optimal frequency ratio of IABI has also decreased

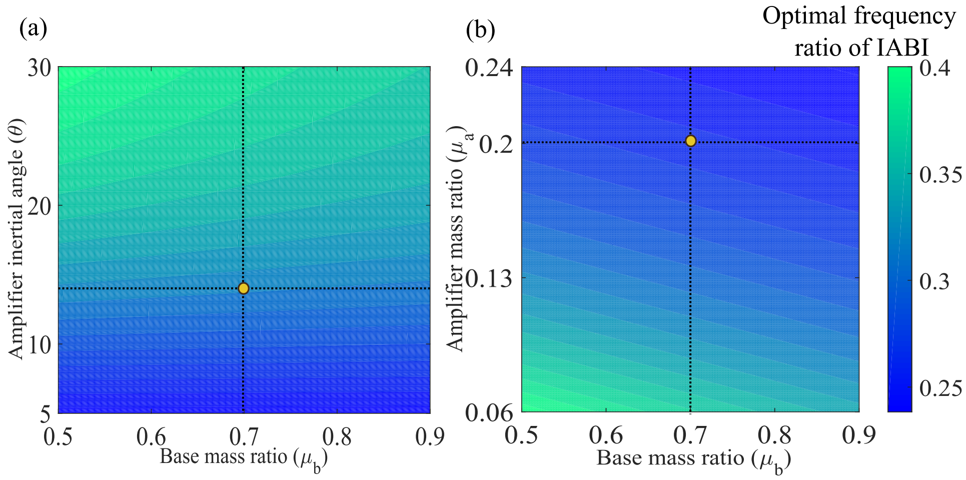

Figure 3. The contour plot of the optimal frequency ratio of IABI ($(\eta_b)_{opt}$) as a function of (a) amplifier inertial angle (θ) and base mass ratio μ_b, (b) amplifier mass ratio (μ_a) and base mass ratio μ_b has been drawn.

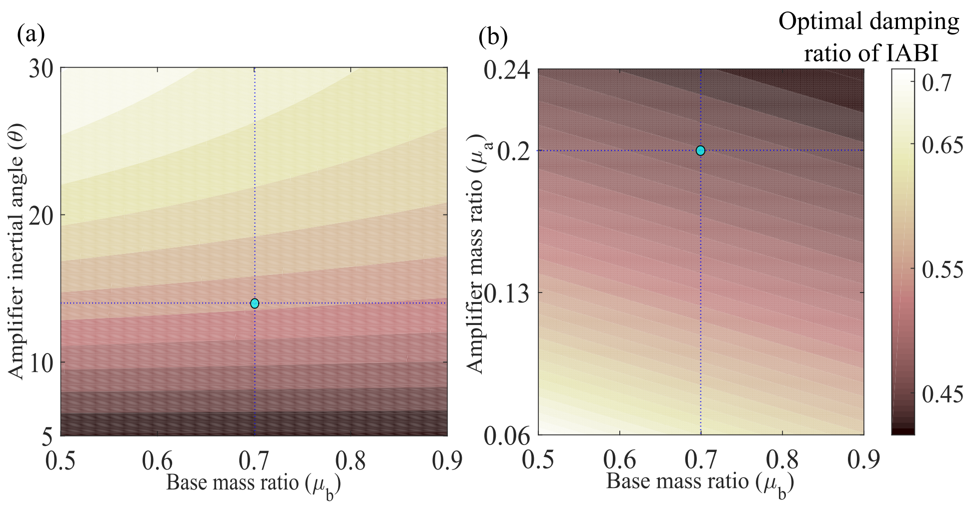

Figure 4. (a) The contour plot of the optimal damping ratio of IABI ($(\zeta_b)_{opt}$) as a function of (a) amplifier inertial angle (θ) and base mass ratio μ_b, (b) amplifier mass ratio (μ_a) and base mass ratio μ_b has been drawn.

when the values of θ decrease. In fact, for $5^o < \theta < 14^o$, the values for frequency ratios are minimum. This phenomenon implies that the lower inertial angle increases the effective mass of the IABI, which provides additional flexibility and enhances the isolated structures' time period. The same trend has also been observed for the

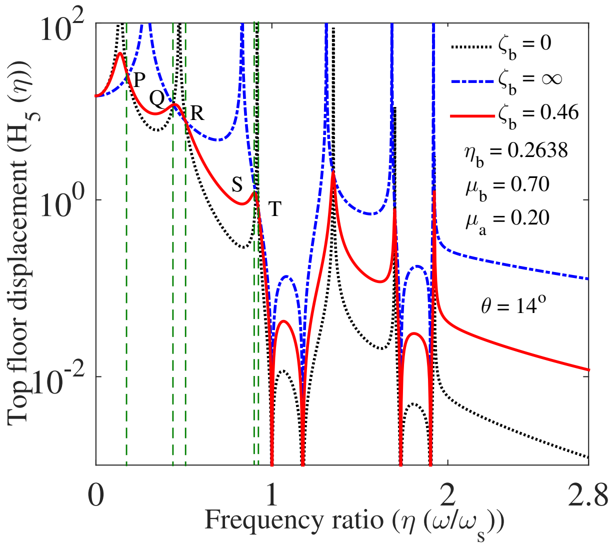

Figure 5. The variations of displacement of top floor $H_5(\eta)$ isolated by inertial amplifier base isolator versus frequency ratio $\eta(\omega/\omega_s)$ have been plotted for different values of damping ratio of the IABI.

closed form equation of optimal viscous damping ratio of IABI. For $5^o < \theta < 14^o$ the values for optimal viscous damping ratios are lower around $0.45 < \zeta_b < 0.55$. These values are feasible and easy for practical implementation. The efficiency of these optimal closed-form expressions is verified by drawing the response graphs in the frequency domain for different values of viscous damping ratio after considering the optimal frequency ratio. Therefore, the robust response plots are shown in Figure 5. For this plot, the system parameters have been considered as $\zeta_s = 0$, $\mu_b = 0.70$ and $\mu_a = 0.20$. The optimal frequency and damping ratios values are applied as 0.2638 and 0.46. From this figure, it can be observed that the response plot of the main structure is unbounded at $\zeta_b = 0$, and the eigen frequencies are located from the response peaks (i.e.,$\eta = 0.1379, 0.4733, 0.9154, 1.349, 1.699, 1.923$). A slight shift of responses has been observed from the eigen frequencies due to the presence of IABI's damping. Most of the response peaks are reduced at resonating frequencies. Hence, the resonance peaks are located at $\eta = 0.1376, 0.4483, 0.9014, 1.348, 1.698, 1.923$. The minimum frequency peaks are located at $\eta = 0.3362, 0.8308, 1.614$ and the anti-resonance frequency region are located at $\eta = 1.0, 1.175, 1.732, 1.902$. At $\zeta_b = \infty$, the total controlled structure becomes over-damped, and the response plot shows that it abbreviates to the uncontrolled structure. The peak response of the top floor of the main structure was determined as 45.23.

4. Dynamic response evaluation of multi-storey buildings

4.1. *Dynamic responses of structures for harmonic and random-white noise excitations*

The variations of top floor displacement of uncontrolled five-storey buildings and controlled five buildings subjected to harmonic base excitation have been displayed in Figure 6 (a). The details of the design parameters for inertial amplifier base isolators and traditional base isolators have been listed in Table.1. The maximum

Table 1. The values of design parameters for uncontrolled buildings and buildings isolated by TBI, IABI. Equation (2.25) and Eq. (2.23) have been utilized to achieve optimal design parameters of IABI and TBI.

TBI	IABI	TBI	IABI
ζ_s	ζ_s	0.01	0.01
ζ_B	ζ_b	0.64	0.46
η_B	η_b	0.39	0.2638
μ_B	$\mu_b + 2\mu_a$	1.1	1.1
$\cdots$	μ_b	0	0.70
$\cdots$	μ_a	0	0.20
$\cdots$	θ	0	14^o

Note: ζ_B=viscous damping ratio of TBI
η_B=Frequency ratio of TBI
μ_B=Base mass ratio of TBI

displacement responses of the top floor of five-storey building isolated by traditional base isolator and inertial amplifier base isolator have been determined as 92.62 and 45.41. From this result, it has been remarked that IABI is significantly 50.97 % superior to TBI. The variations of top floor displacement of uncontrolled five-storey buildings and controlled five buildings subjected to random base excitation have been displayed in Figure 6 (b). The maximum displacement responses of the top floor of five-storey building isolated by traditional base isolator and inertial amplifier base isolator subjected to random vibrations have been determined as 1.525×10^8 dB/Hz and 3.709×10^7 dB/Hz. Therefore, the vibration reduction capacity of IABI is significantly 75.67 % superior to TBI.

4.2. *Time history analysis*

The numerical study has validated the results obtained from the frequency-domain analysis and the optimal closed-form expressions by considering real earthquake base excitations. The governing equations of motion have been solved in the MATLAB environment by coding the Newmark-beta method. The details of the design

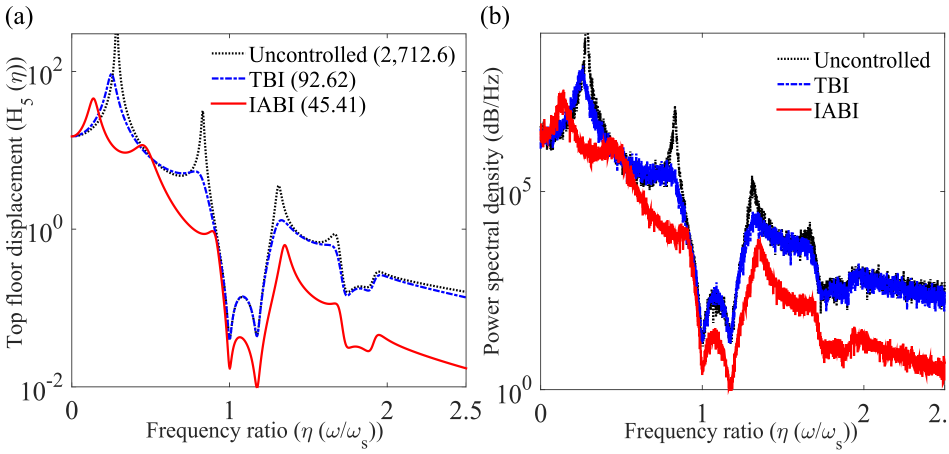

Figure 6. The variations of displacement of the top floor of the five-storey building isolated by H_2 optimized traditional base isolator and inertial amplifier base isolator have been displayed for (a) harmonic and (b) random base excitation.

parameters for this analysis have already been listed in Table.1. The structural damping ζ_s considers as 0.01. The mass of each floor m_s considers as 3000 tons and the structural time period T_s considers as 0.5 sec.

To perform this numerical analysis, eleven near-field real earthquake records have been downloaded from the Pacific Earthquake Engineering Research Center (https://peer.berkeley.edu/peer-strong-ground-motion-databases) and applied in the MATLAB codes to determine the dynamic responses of the structures. The detailed properties of near-field earthquake records have been listed in Table.2. The

Table 2. Details of near-field earthquake ground motions (Pulse records).

Earthquake	Year	M_w	Recording station	Vs_{30}(m/s)	Component	E_s (km)	PGA,g
Irpinia, Italy-01	1980	6.9	Sturno	1000	MUL009	30.4	0.31
Superstition Hills-02	1987	6.5	Parachute Test Site	349	SUPERST	16.0	0.42
Loma Prieta	1989	6.9	LOMAP	371	HEC000	27.2	0.38
Erzican, Turkey	1992	6.7	Erzincan 11	275	ERZIKAN	9.0	0.49
Cape Mendocino	1992	7.0	CAPEMEND	713	NIS090	4.5	0.63
Landers	1992	7.3	Lucerne	685	LANDERS	44.0	0.79
Northridge-01	1994	6.7	Rinaldi Receiving Sta	282	NORTHR	10.9	0.87
Kocaeli, Turkey	1999	7.5	Izmit	811	KOCAELI	5.3	0.22
Chi-Chi, Taiwan	1999	7.6	TCU065	306	CHICHI	26.7	0.82
Chi-Chi, Taiwan	1999	7.6	TCU102	714	CHICHI	45.6	0.29
Duzce, Turkey	1999	7.1	Duzce	276	DUZCE	1.6	0.52

response spectra of considered earthquakes for 5% damping are shown in Figure 7. The near-field earthquakes are more vulnerable compared to the far-field earthquakes [31,50,51]. Therefore, the study has continued near-field earthquake records

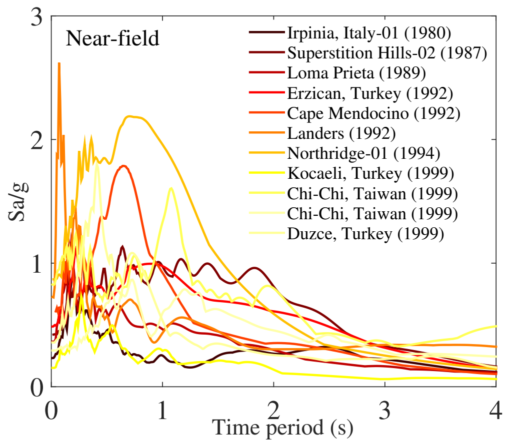

Figure 7. Response spectra of earthquake base excitations.

with pulses having a noticeable vertical component, which is more harmful to the base-isolated structures. The variations of top floor displacements for Cape Mendocino, Northridge-01, Chi-Chi, Taiwan near-field earthquake earthquake base excitations have been shown in Figure 8 (a), Figure 8 (b), and Figure 8 (c). The details of maximum displacement of top floor for controlled and uncontrolled five-storey buildings have been listed in Table.3. IABI effectively reduces the top floor displacement of the multi storey buildings, and overall, the displacement reduction capacity of IABI is significantly 49.03% superior to the displacement reduction capacity of TBI. Table.3 also shows the displacement reduction capacity of IABI

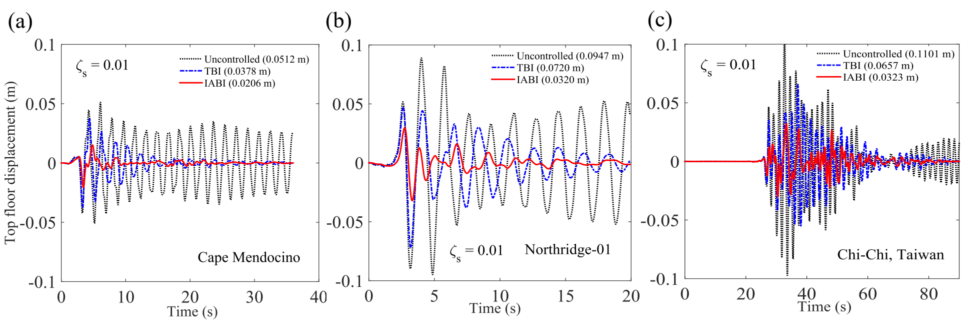

Figure 8. The variations of top floor displacement for (a) Cape Mendocino, (b) Northridge-01, (c) Chi-Chi, Taiwan near-field earthquake earthquake base excitations.

relative to TBI ($D_r(\%)$) for five-story buildings subjected to near-field earthquake ground motions.

Table 3. Top floor maximum displacement responses x_5^{max} (m) with corresponding displacement reduction of IABI w.r.t TBI ($D_r(\%)$) under near-field earthquake ground motions for five-storey buildings.

Earthquakes	Uncontrolled structures x_5^{max} (m)	TBI x_5^{max} (m)	IABI x_5^{max} (m)	$D_r(\%)$
Irpinia, Italy-01	0.0456	0.0246	0.0122	50.41
Superstition Hills-02	0.1515	0.0788	0.0264	66.50
Loma Prieta	0.0577	0.0297	0.0151	49.16
Erzican, Turkey	0.0844	0.0594	0.027	54.55
Cape Mendocino	0.0512	0.0378	0.0206	45.50
Landers	0.0322	0.0321	0.028	12.77
Northridge-01	0.0947	0.072	0.032	55.56
Kocaeli, Turkey	0.0323	0.0133	0.0057	57.14
Chi-Chi, Taiwan	0.1101	0.0657	0.0323	50.84
Chi-Chi, Taiwan	0.0898	0.0433	0.0196	54.73
Duzce, Turkey	0.0449	0.0237	0.0137	42.19
Average	0.0722	0.0437	0.0211	49.03

$$D_r(\%) = \frac{(x_5^{max})_{TBI} - (x_5^{max})_{IABI}}{(x_5^{max})_{TBI}} \tag{4.1}$$

The variations of top floor accelerations for Cape Mendocino, Northridge-01, Chi-Chi, Taiwan near-field earthquake earthquake base excitations have been shown in Figure 9 (a), Figure 9 (b), and Figure 9 (c). The details of maximum acceleration of top floor for controlled and uncontrolled five-storey buildings have been listed in Table.4. IABI effectively reduces the top floor acceleration of the multi storey buildings, and overall, the acceleration reduction capacity of IABI is significantly 56.02% superior to the acceleration reduction capacity of TBI. Table.4 also shows

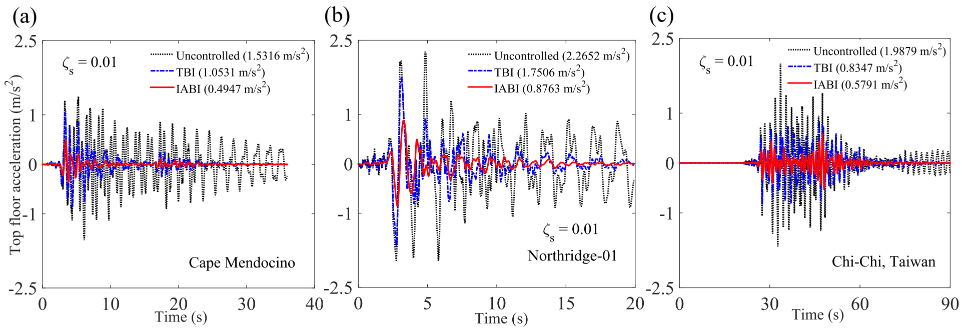

Figure 9. The variations of top floor acceleration for (a) Cape Mendocino, (b) Northridge-01, (c) Chi-Chi, Taiwan near-field earthquake earthquake base excitations.

the acceleration reduction capacity of IABI relative to TBI ($A_r(\%)$) for five-story buildings subjected to near-field earthquake ground motions.

Table 4. Top floor maximum acceleration responses $\ddot{x}_5^{max}$ (m/s^2) with corresponding acceleration reduction of IABI w.r.t TBI ($A_r(\%)$) under near-field earthquake ground motions for five-storey buildings.

Earthquakes	Uncontrolled structures $\ddot{x}_5^{max}$ (m/s^2)	TBI $\ddot{x}_5^{max}$ (m/s^2)	IABI $\ddot{x}_5^{max}$ (m/s^2)	$A_r(\%)$
Irpinia, Italy-01	0.6848	0.3225	0.11	65.89
Superstition Hills-02	2.03	1.0428	0.3489	66.54
Loma Prieta	0.8702	0.6544	0.2346	64.15
Erzican, Turkey	1.4185	1.1978	0.5004	58.22
Cape Mendocino	1.5316	1.0531	0.4947	53.02
Landers	0.9191	0.5761	0.233	59.55
Northridge-01	2.2652	1.7506	0.8763	49.94
Kocaeli, Turkey	0.6358	0.3054	0.1017	66.69
Chi-Chi, Taiwan	1.9879	0.8347	0.5791	30.62
Chi-Chi, Taiwan	1.6006	0.5434	0.3113	42.71
Duzce, Turkey	0.7833	0.6003	0.2466	58.92
Average	1.338	0.807	0.366	56.02

$$A_r(\%) = \frac{(\ddot{x}_5^{max})_{TBI} - (\ddot{x}_5^{max})_{IABI}}{(\ddot{x}_5^{max})_{TBI}} \tag{4.2}$$

Based on Table.3 and Table.4, two bar diagrams have been drawn and presented in Figure 10 (a) and Figure 10 (b) to display the normalized maximum displacement and acceleration of the main structure's top floor subjected to near-field earthquake base excitations. The average displacement of uncontrolled structures for

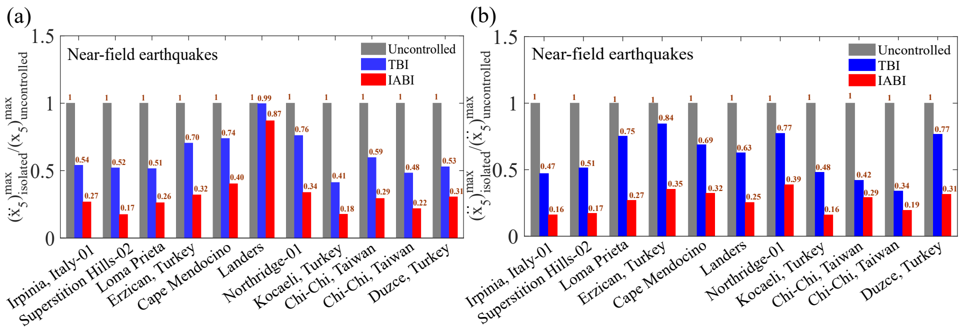

Figure 10. The normalized (a) maximum displacement and (b) maximum acceleration of the main structure's top floor subjected near-field earthquake base excitations.

eleven near-field earthquake records has been obtained as 0.0722 m. The average displacement of structures isolated by TBI and IABI for eleven near-field earthquake records have been obtained as 0.0437 m and 0.0211 m. Therefore, results show that the displacement reduction capacity (%) of IABI is significant 49.03 % superior to the displacement reduction capacity (%) of TBI subjected to near-field base excitations. The average acceleration of uncontrolled structures for eleven near-field earthquake records has been obtained as 1.338 m/s^2. The average acceleration of structures isolated by TBI and IABI for eleven near-field earthquake records have been obtained as 0.807 m/s^2 and 0.366 m/s^2. Results show that the acceleration reduction capacity (%) of IABI is significant 56.02 % superior to the displacement reduction capacity (%) of TBI subjected to near-field base excitations. The damping force-deformation curves of the top floors of the uncontrolled and controlled buildings subjected to Cape Mendocino, Northridge-01, Chi-Chi, Taiwan near-field earthquake earthquake base excitations are shown in Figure 11 (a), Figure 11 (b), and Figure 11 (c). Figure 11 displays the damping force-deformation curves of the top floor damping force having viscous damping ratio of each floor ζ_s as 0.01, in which the maximum displacement of the top floor and maximum damping force of the five-storey building isolated by IABI are underneath than those of the uncontrolled five-storey buildings. The damping force reduction in IABI controlled

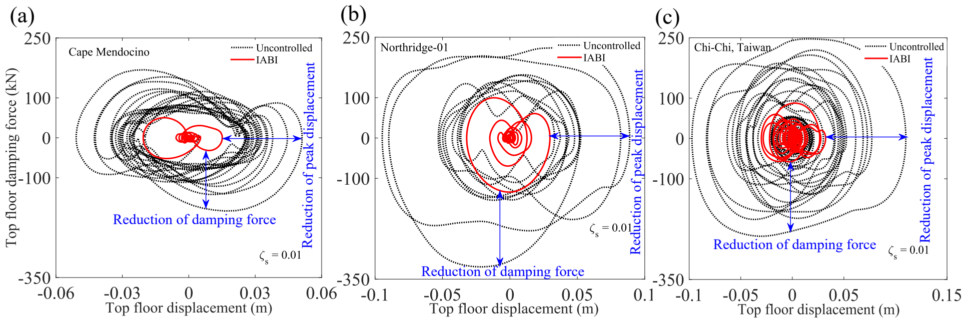

Figure 11. The damping force-deformation curves of the top floor of the uncontrolled and controlled buildings subjected to (a) Cape Mendocino, (b) Northridge-01, (c) Chi-Chi, Taiwan near-field earthquake earthquake base excitations.

structure can clearly visible from Figure 11. The variations of maximum displacement of each floor of uncontrolled and controlled five-storey buildings subjected to Cape Mendocino, Northridge-01, Chi-Chi, Taiwan near-field earthquake base excitations w.r.t floor levels have been displayed in Figure 12 (a), Figure 12 (b), and Figure 12 (c). It is observed that both TBI and IABI lead to a significant reduction of the displacement responses for each floor compared to the uncontrolled structure. Overall, IABI has 51.07% more displacement reduction capacity than TBI under near-field earthquake base excitations in terms of all floor responses. The variations of maximum acceleration of each floor of uncontrolled and controlled five-storey buildings subjected to Cape Mendocino, Northridge-01, Chi-Chi, Taiwan near-field earthquake base excitations w.r.t floor levels have been displayed in Figure 12 (d), Figure 12 (e), and Figure 12 (f). It is observed that both TBI and IABI lead to a significant reduction of the acceleration responses of each floor compared to the uncontrolled structure. Between IABI and TBI, the acceleration reduction capac-

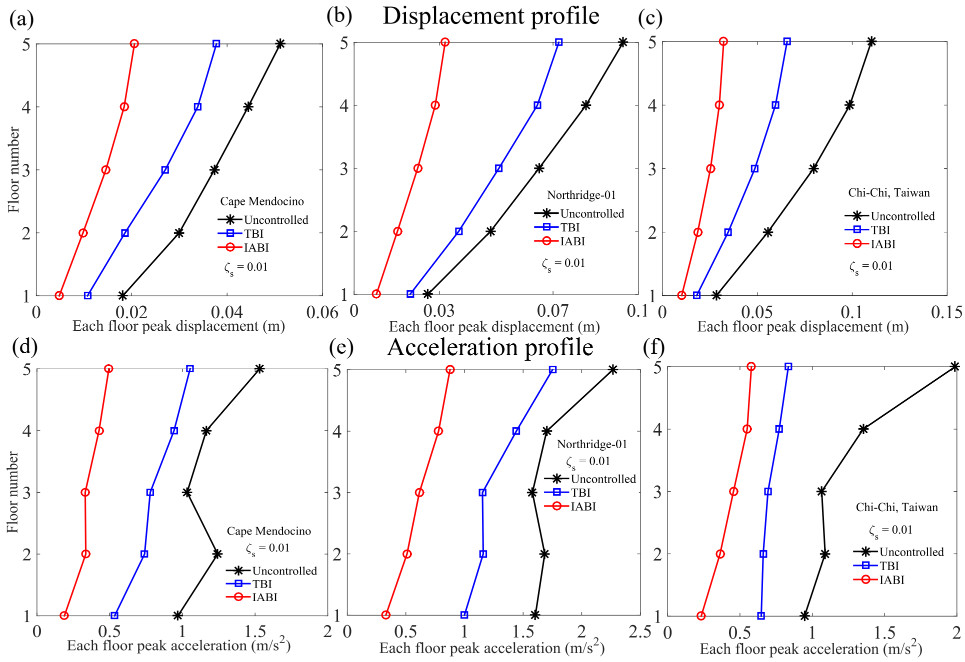

Figure 12. The variations of maximum displacement of each floor of uncontrolled and controlled five-storey buildings w.r.t floor levels have been displayed for (a) Cape Mendocino, (b) Northridge-01, (c) Chi-Chi, Taiwan near-field earthquake base excitations. The variations of maximum acceleration of each floor of uncontrolled and controlled five-storey buildings w.r.t floor levels have been displayed. (d) Cape Mendocino, (e) Northridge-01, (f) Chi-Chi, Taiwan near-field earthquake records have been selected to draw these performance plots.

ity of IABI is the most. For more technical illustration, the exact values of the acceleration reduction capacity (%) for each floor considering Cape Mendocino, Northridge-01, Chi-Chi, Taiwan near-field earthquakes have been described. Overall, IABI has 51.53% more acceleration reduction capacity than TBI subjected to near-field earthquake base excitations. The energy flow between the uncontrolled structure and structure isolated by TBI, IABI, needs to be determined. Therefore, the variations of normalized energies of uncontrolled structure and structure isolated by TBI and IABI versus time (s) subjected to Northridge-01 earthquake base excitations have been shown in Figure 13 (a), Figure 13 (b), and Figure 13 (c). The kinetic, potential, and dissipated energy profiles of uncontrolled structures are much higher than the energy profile of structures isolated by TBI and IABI. Hence, the main structural energies are transferred to the isolators during vibrations. The energies are dissipated through the isolators, respectively. The energy profile of the structure isolated by TBI is much higher than that of IABI. Therefore, the energy dissipation and response mitigation capacity of IABI are significantly superior to the TBI, respectively.

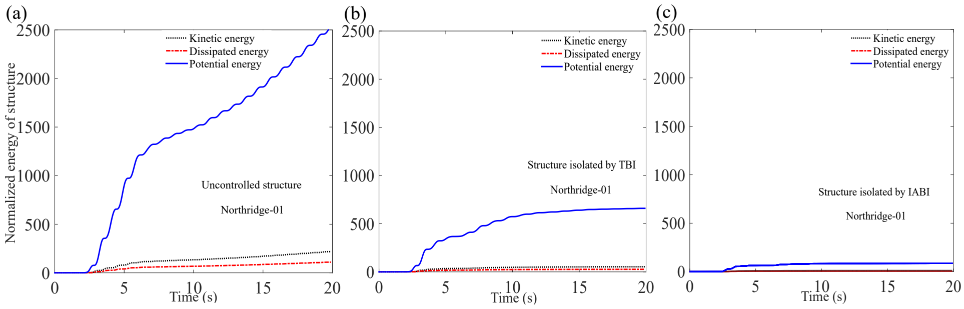

Figure 13. The variations of normalized energies of (a) uncontrolled structure and structure isolated by (b) TBI and (c) IABI versus time (s) subjected to Northridge-01 earthquake base excitations.

5. Vibration reduction capacity of IABI as per floor levels

The variations of top floor displacement of uncontrolled ten-storey buildings and ten-storey buildings isolated by TBI, IABI subjected to harmonic base excitation have been displayed in Figure 14 (a). The maximum displacement responses of the top floor of ten-storey building isolated by traditional base isolator and inertial amplifier base isolator have been determined as 1315.70 and 296.86. Hence, the response reduction capacity of H_2 optimized IABI for ten-storey buildings is significantly 77.43 % superior to H_2 optimized TBI. The variations of top floor

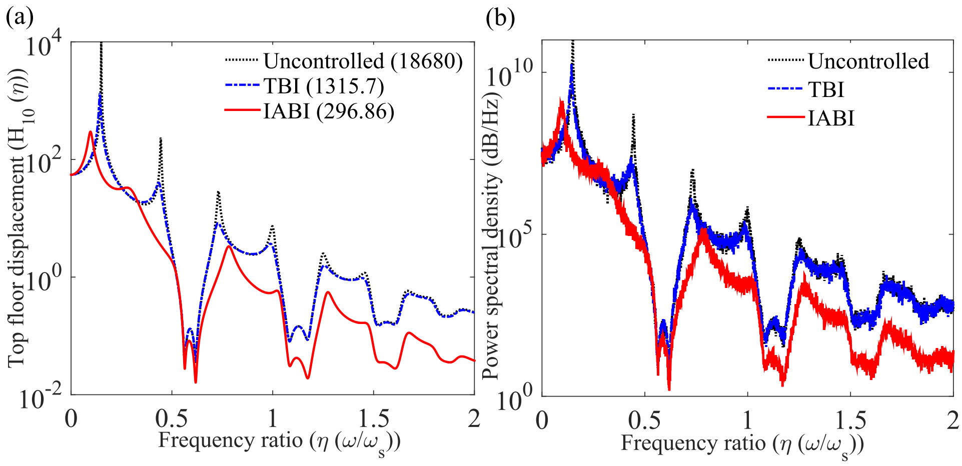

Figure 14. The variations of displacement of the top floor of the ten-storey building $H_{10}(\eta)$ isolated by H_2 optimized traditional base isolator and inertial amplifier base isolator have been displayed for (a) harmonic and (b) random base excitation.

displacement of uncontrolled ten-storey buildings and ten-storey buildings isolated by traditional base isolator, inertial amplifier base isolator subjected to Gaussian white noise base excitation have been displayed in Figure 14 (b). Results shows that the response reduction capacity of IABI is significantly 93.86 % superior to TBI under white-noise random excitation. The accuracy of frequency domain results and optimal closed-form expressions have also be verified by the numerical study. The structural damping for each floor considers 0.01. Total isolator mass ratios for TBI and IABI are considered 1.1. The inertial angle considers as 14^o. The frequency ratios for IABI and TBI are considered as 0.2638 and 0.39. The viscous ratios for IABI and TBI are considered 0.46 and 0.64. For the numerical study, the time period of the buildings considers as $T_s = 1.0$ sec. Hence, the natural frequency of the building has been derived as $\omega_s = \frac{2\pi}{T_s}$. Each floor's mass is considered $m_s = 3000$ tons. For this study, Northridge-01 near-field earthquake base excitation has been induced. Figure 15 (a) shows the variations of top floor displacement (m) of uncontrolled ten-storey building and ten-storey buildings isolated by TBI, IABI subjected to Northridge-01 near-field earthquake base excitation. The displacement reduction capacity of IABI has been determined and is significantly 43.07 % superior to the displacement reduction capacity of TBI. Simultaneously, the variations of top floor

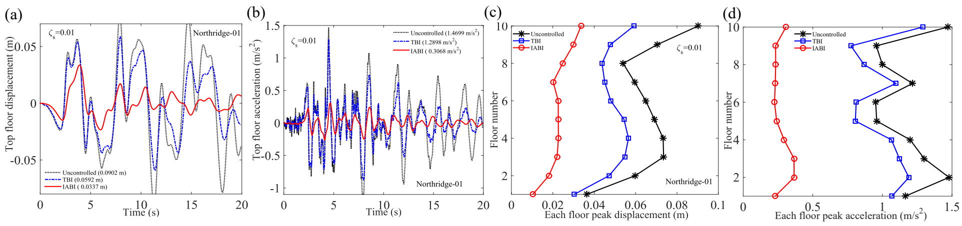

Figure 15. The variations of top floor (a) displacement (m), (b) acceleration (m/s^2), (c) maximum displacement (m) of each floor, and (d) maximum acceleration (m/s^2) of each floor of ten-storey uncontrolled buildings and ten-storey buildings isolated by TBI and IABI subjected to Northridge-01 near-field base excitation.

acceleration (m/s^2) of uncontrolled and controlled ten-storey buildings isolated by TBI and IABI subjected to Northridge-01 near-field earthquake base excitation have been displayed in Figure 15 (b). The acceleration reduction capacity of IABI is significantly 76.21 % superior to the acceleration reduction capacity of TBI. The variations of maximum displacement of each floor of uncontrolled and controlled ten-storey buildings under Northridge-01 near-field earthquake base excitation w.r.t floor levels have been displayed in Figure 15 (c). The average displacement reduction of IABI over the displacement reduction TBI has been achieved as 53.39 %, respectively. Figure 15 (d) shows the variations of top floor acceleration (m/s^2) of uncontrolled ten-storey building and ten-storey buildings isolated by TBI, IABI subjected to Northridge-01 near-field earthquake base excitation. The acceleration reduction capacity of IABI is significantly 73.02 % superior to the acceleration reduction capacity of TBI. Figure 16 displays the force-deformation curves of the top floor damping force having viscous damping ratio of each floor ζ_s as 0.01, in which the maximum displacement of the top floor and maximum damping force of the ten-storey building isolated by IABI are underneath than those of the uncontrolled ten-storey buildings. The vibration reduction capacity of IABI has been investi-

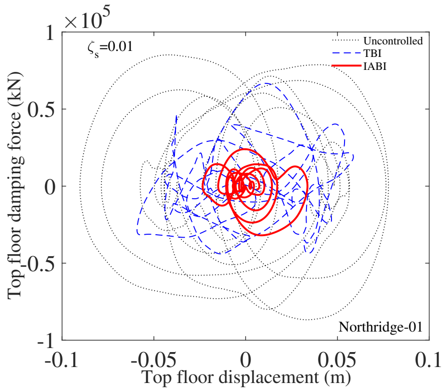

Figure 16. The damping force-deformation curves of the top floor of the uncontrolled and controlled buildings subjected to Northridge-01 near-field earthquake base excitation.

gated for acceleration control range and velocity control range buildings. The class of building is determined based on the building's time period, which predominantly depends on the number of stories. In the response spectrum, time periods less than 0.6 s and between 0.6 s and 4 s are classified as the acceleration and velocity control range. Because a building's time period is approximately 0.1 times its number of stories, five- and ten-story buildings are in the acceleration and velocity control case. These two examples are used to demonstrate that the proposed isolators performed well in both building categories. From the current study it has been observed that the vibration reduction capacity of traditional base isolators decreases critically while the floor level of multi-storey buildings increases mainly beyond 10 storeys. However, IABI still efficiently mitigates displacement and acceleration responses under near-field earthquake base excitations. The damping force reduction by IABI is also effective. IABI is also effective for beyond 10 storeys.

6. Summary and conclusions

The vibration reduction capacity of optimum IABI for multi-storey buildings have been investigated in this paper. One of the notable contributions of this paper is the new closed-form expressions for optimal design parameters of inertial amplifier base isolator (IABI) for multi-storey buildings, which have been derived using H_2 optimization method. Initially, the dynamic responses of multi-storey buildings isolated by optimum IABI and TBI subjected to harmonic and random-white noise have been determined. Later, the efficiency of H_2 optimized design parameters such as frequency and viscous damping ratio have been scrutinized by the time history analysis considering eleven near-field earthquake base excitations. The significant results are listed below.

- The higher base mass with a lower amplifier's inertial angle and higher amplifier's mass ratio of IABI has been recommended to design the optimal IABI to achieve robust vibration reduction capacity.
- Results from the five-storey buildings showed that the vibration reduction capacity of optimum IABI is significantly 50.97 % and 75.67 % superior to the optimum TBI under harmonic and white-noise random base excitations. The numerical study shows that optimum IABI has 49.03% more displacement reduction capacity than optimum TBI under near-field earthquake base excitations. At the same time, IABI has 56.02% more acceleration reduction capacity than TBI.
- Later, H_2 optimized design parameters have been applied for ten-storey buildings. Results show that the vibration reduction capacity of H_2 optimized IABI is significantly 77.43 % and 93.86 % superior to H_2 optimized TBI under harmonic and white-noise random base excitations.
- The numerical study shows that H_2 optimized IABI has 43.07 % more displacement reduction capacity than H_2 optimized TBI. At the same time, H_2 optimized IABI has 76.21 % more acceleration reduction capacity than H_2 optimized TBI.
- Results show that IABI is very efficient in reducing the vertical components of earthquake base excitations, especially for near-field earthquake base excitations with the pulse nature.
- The vibration reduction capacity of traditional base isolators decreases critically while the floor level of multi-storey buildings increases mainly beyond 10 storeys. However, IABI still efficiently mitigates displacement and acceleration responses under near-field earthquake base excitations. The damping force reduction by IABI is also effective. IABI is also effective for beyond 10 storeys.

The paper's novelty lies in proposing inertial amplifier base isolators for vibration attenuation of multi-storey buildings, which is not there in state of the art based on the author's best knowledge. Additionally, the proposition of the new closed-form expressions for optimal design parameters of the inertial amplifier base isolators is another critical contribution of this paper. These equations resulted in the optimal design of these isolators, resulting in the maximum amount of vibration reduction. The novel inertial amplifier base isolators are cost-effective and dissipate more energy than the traditional base isolators without increasing the static mass. As suggested by the coauthors, a continuation of the present work with an emphasis on the practical realization, experimentation, and prototyping of the proposed inertial amplifier base isolators will be carried out.

Declaration of competing interest

The authors declare that they have no known competing financial interests or personal relationships that could have appeared to influence the work reported in this paper

Acknowledgement

The authors' would like to acknowledge the Inspire faculty grant, grant number DST/ INSPIRE/04/2018/000052 for partial financial support for the project. SC would like to acknowledge the MHRD grant received from IIT Delhi during the period of this research work.

References

1. Z. Li, G. Huang, X. Chen and X. Zhou, Seismic response and parametric analysis of inter-story isolated tall buildings based on enhanced simplified dynamic model, *International Journal of Structural Stability and Dynamics* **22**(03n04) (2022) p. 2240008.
2. S. Zhang, Y. Hu, X. Liu, P. Tan and X. Guo, Hybrid isolation strategy for seismically isolated multi-tower building with a large podium, *International Journal of Structural Stability and Dynamics* **22**(06) (2022) p. 2250061.
3. B. Soneji and R. Jangid, Effectiveness of seismic isolation for cable-stayed bridges, *International Journal of Structural Stability and Dynamics* **6**(01) (2006) 77–96.
4. A. E. Taha, S. Elias, V. Matsagar and A. K. Jain, Seismic response control of asymmetric buildings using tuned mass dampers, *The Structural Design of Tall and Special Buildings* **28**(18) (2019) p. e1673.
5. J. Love, B. Morava and A. Smith, Monitoring of a tall building equipped with an efficient multiple-tuned sloshing damper system, *Practice Periodical on Structural Design and Construction* **25**(3) (2020) p. 05020003.
6. A. Das, D. Maity and S. K. Bhattacharyya, Investigation on the efficiency of deep liquid tanks in controlling dynamic response of high-rise buildings: A computational framework, *Structures* **37** (2022) 1129–1141.
7. T. Konar and A. D. Ghosh, Adaptation of a deep liquid-containing tank into an effective structural vibration control device by a submerged cylindrical pendulum appendage, *International Journal of Structural Stability and Dynamics* **21**(06) (2021) p. 2150078.
8. H. Han, V. Sorokin, L. Tang and D. Cao, Lightweight origami isolators with deployable mechanism and quasi-zero-stiffness property, *Aerospace Science and Technology* **121** (2022) p. 107319.
9. X.-X. Bai, P. Jiang and L.-J. Qian, Integrated semi-active seat suspension for both longitudinal and vertical vibration isolation, *Journal of Intelligent Material Systems and Structures* **28**(8) (2017) 1036–1049.
10. M. Shrimali and R. Jangid, A comparative study of performance of various isolation systems for liquid storage tanks, *International Journal of Structural Stability and Dynamics* **2**(04) (2002) 573–591.
11. M. Furinghetti, A. Pavese, V. Quaglini and P. Dubini, Experimental investigation of the cyclic response of double curved surface sliders subjected to radial and bidirectional sliding motions, *Soil Dynamics and Earthquake Engineering* **117** (2019) 190–202.
12. M. Furinghetti, I. Lanese and A. Pavese, Experimental assessment of the seismic response of a base-isolated building through a hybrid simulation technique, *Frontiers in Built Environment* **6** (2020) p. 33.

13. M. Furinghetti, T. Yang, P. M. Calvi and A. Pavese, Experimental evaluation of extra-stroke displacement capacity for curved surface slider devices, *Soil Dynamics and Earthquake Engineering* **146** (2021) p. 106752.
14. A. Das, D. Maity and S. K. Bhattacharyya, Characterization of liquid sloshing in u-shaped containers as dampers in high-rise buildings, *Ocean Engineering* **210** (2020) p. 107462.
15. T. Sheng, G.-b. Liu, X.-c. Bian, W.-x. Shi and Y. Chen, Development of a three-directional vibration isolator for buildings subject to metro-and earthquake-induced vibrations, *Engineering Structures* **252** (2022) p. 113576.
16. Y. Wen and B. Hui, Stochastic optimization of multiple tuned inerter dampers for mitigating seismic responses of bridges with friction pendulum systems, *International Journal of Structural Stability and Dynamics* **22**(13) (2022) p. 2250137.
17. C. Han, B.-H. Kang, S.-B. Choi, J. M. Tak and J.-H. Hwang, Control of landing efficiency of an aircraft landing gear system with magnetorheological dampers, *Journal of Aircraft* **56**(5) (2019) 1980–1986.
18. F. Liu, D. Yu, C. Wang and G. Wang, Advances in variable stiffness vibration isolator and its application in spacecraft, *International Journal of Structural Stability and Dynamics* (2022) p. 2230004.
19. M. C. Chen, J. I. Restrepo, C. Blandon and J. F. Velásquez, Performance-based seismic design framework for inertia-sensitive nonstructural components in base-isolated buildings, *Journal of Building Engineering* **43** (2021) p. 103073.
20. D. Losanno, N. Ravichandran and F. Parisi, Seismic fragility of base-isolated single-storey unreinforced masonry buildings equipped with classical and recycled rubber bearings in himalayan regions, *Journal of Building Engineering* **45** (2022) p. 103648.
21. X. B. Nguyen, T. Komatsuzaki and H. T. Truong, Adaptive parameter identification of bouc-wen hysteresis model for a vibration system using magnetorheological elastomer, *International Journal of Mechanical Sciences* **213** (2022) p. 106848.
22. P. Sheng, S. Jing and Z. Zhang, On the characteristics and practical parameters selection of a quasi-zero-stiffness isolator, *International Journal of Structural Stability and Dynamics* **0**(0) (0) p. 2250172.
23. H. Li, C. Yang, S. Wang, P. Su, Y. Zhu, X. Zhang, Z. Peng and Q. Mu, Study on the nonlinear dynamic characteristics of spherical rubber isolators by experiments and simulations based on harmonic balance method, *International Journal of Structural Stability and Dynamics* **22**(11) (2022) p. 2250133.
24. I. G. Buckle, New zealand seismic base isolation concepts and their application to nuclear engineering, *Nuclear Engineering and Design* **84**(3) (1985) 313–326.
25. W. H. Robinson, Lead-rubber hysteretic bearings suitable for protecting structures during earthquakes, *Earthquake engineering & structural dynamics* **10**(4) (1982) 593–604.
26. R. Jangid, Computational numerical models for seismic response of structures isolated by sliding systems, *Structural Control and Health Monitoring* **12**(1) (2005) 117–137.
27. R. Jangid, Optimum friction pendulum system for near-fault motions, *Engineering Structures* **27**(3) (2005) 349–359.
28. J. Zhang, Y. Ding and X. Guan, Overturning resistance of friction pendulum bearing-isolated structure subjected to impact, *International Journal of Structural Stability and Dynamics* **22**(06) (2022) p. 2250072.
29. H. Shakib and A. Fuladgar, Response of pure-friction sliding structures to three components of earthquake excitation, *Computers & Structures* **81**(4) (2003) 189–196.
30. M. Z. Chen and Y. Hu, Analysis for inerter-based vibration system, in *Inerter and Its Application in Vibration Control Systems* (Springer, 2019), pp. 19–39.

31. S. Chowdhury and A. Banerjee, The exact closed-form expressions for optimal design parameters of resonating base isolators, *International Journal of Mechanical Sciences* **224** (2022) p. 107284.
32. Z. Cheng, A. Palermo, Z. Shi and A. Marzani, Enhanced tuned mass damper using an inertial amplification mechanism, *Journal of Sound and Vibration* **475** (2020) p. 115267.
33. S. R. Patro, A. Banerjee, S. Adhikari and G. Ramana, Kaimal spectrum based h2 optimization of tuned mass dampers for wind turbines, *Journal of Vibration and Control* (2022) p. 10775463221092838.
34. M. Baduidana and A. Kenfack-Jiotsa, Optimal design of inerter-based isolators minimizing the compliance and mobility transfer function versus harmonic and random ground acceleration excitation, *Journal of Vibration and control* **27**(11-12) (2021) 1297–1310.
35. D. Čakmak, Z. Tomičević, H. Wolf, Ž. Božić and D. Semenski, Stability and performance of supercritical inerter-based active vibration isolation systems, *Journal of Sound and Vibration* (2021) p. 116234.
36. Y. Hu and M. Z. Chen, Performance evaluation for inerter-based dynamic vibration absorbers, *International Journal of Mechanical Sciences* **99** (2015) 297–307.
37. F. Qian, Y. Luo, H. Sun, W. C. Tai and L. Zuo, Optimal tuned inerter dampers for performance enhancement of vibration isolation, *Engineering Structures* **198** (2019) p. 109464.
38. M. C. Smith and F.-C. Wang, Performance benefits in passive vehicle suspensions employing inerters, *Vehicle system dynamics* **42**(4) (2004) 235–257.
39. Z. Zhao, Q. Chen, R. Zhang, C. Pan and Y. Jiang, Optimal design of an inerter isolation system considering the soil condition, *Engineering Structures* **196** (2019) p. 109324.
40. R. Zhang, Z. Zhao and C. Pan, Influence of mechanical layout of inerter systems on seismic mitigation of storage tanks, *Soil Dynamics and Earthquake Engineering* **114** (2018) 639–649.
41. C. Yilmaz, G. M. Hulbert and N. Kikuchi, Phononic band gaps induced by inertial amplification in periodic media, *Physical Review B* **76**(5) (2007) p. 054309.
42. C. Yilmaz and G. Hulbert, Theory of phononic gaps induced by inertial amplification in finite structures, *Physics Letters A* **374**(34) (2010) 3576–3584.
43. A. Banerjee, R. Das and E. P. Calius, Waves in structured mediums or metamaterials: a review, *Archives of Computational Methods in Engineering* **26**(4) (2019) 1029–1058.
44. S. Adhikari and A. Banerjee, Enhanced low-frequency vibration energy harvesting with inertial amplifiers, *Journal of Intelligent Material Systems and Structures* (2021) p. 1045389X211032281.
45. A. Banerjee, S. Adhikari and M. I. Hussein, Inertial amplification band-gap generation by coupling a levered mass with a locally resonant mass, *International Journal of Mechanical Sciences* **207** (2021) p. 106630.
46. G. P. Cimellaro, M. Domaneschi and G. Warn, Three-dimensional base isolation using vertical negative stiffness devices, *Journal of Earthquake Engineering* **24**(12) (2020) 2004–2032.
47. Y. Mi and X. Yu, Sound transmission of acoustic metamaterial beams with periodic inertial amplification mechanisms, *Journal of Sound and Vibration* **499** (2021) p. 116009.
48. S. Chowdhury, A. Banerjee and S. Adhikari, Enhanced seismic base isolation using inertial amplifiers, *Structures* **33** (2021) 1340–1353.
49. S. Chowdhury, A. Banerjee and S. Adhikari, Optimal negative stiffness inertial-

amplifier-base-isolators: Exact closed-form expressions, *International Journal of Mechanical Sciences* (2022) p. 107044.

50. P. Chen, B. Wang, K. Dai and T. Li, Analytical and numerical investigations of base isolation system with negative stiffness devices, *Engineering Structures* **268** (2022) p. 114799.
51. B. L. Khan, M. Azeem, M. Usman, S. H. Farooq, A. Hanif and M. Fawad, Effect of near and far field earthquakes on performance of various base isolation systems, *Procedia Structural Integrity* **18** (2019) 108–118.

Appendix A. Formulation for determining standard deviation of responses

$$\int_{-\infty}^{\infty} \frac{\Xi_n(\omega)\,\mathrm{d}\omega}{\Lambda_n(\mathrm{i}\omega)\Lambda_n^*(\mathrm{i}\omega)} = \frac{\pi}{a_{12}} \frac{\det[\mathbf{N}_{12}]}{\det[\mathbf{D}_{12}]} \tag{A.1}$$

$$N_n = \begin{bmatrix} b_{11} & b_{10} & b_9 & b_8 & b_7 & b_6 & b_5 & b_4 & b_3 & b_2 & b_1 & b_0 \\ -a_{12} & a_{10} & -a_8 & a_6 & -a_4 & a_2 & -a_0 & 0 & 0 & 0 & 0 & 0 \\ 0 & -a_{11} & a_9 & -a_7 & a_5 & -a_3 & a_1 & 0 & 0 & 0 & 0 & 0 \\ 0 & a_{12} & -a_{10} & a_8 & -a_6 & a_4 & -a_2 & a_0 & 0 & 0 & 0 & 0 \\ 0 & 0 & a_{11} & -a_9 & a_7 & -a_5 & a_3 & -a_1 & 0 & 0 & 0 & 0 \\ 0 & 0 & -a_{12} & a_{10} & -a_8 & a_6 & -a_4 & a_2 & -a_0 & 0 & 0 & 0 \\ 0 & 0 & 0 & -a_{11} & a_9 & -a_7 & a_5 & -a_3 & a_1 & 0 & 0 & 0 \\ 0 & 0 & 0 & a_{12} & -a_{10} & a_8 & -a_6 & a_4 & -a_2 & a_0 & 0 & 0 \\ 0 & 0 & 0 & 0 & a_{11} & -a_9 & a_7 & -a_5 & a_3 & -a_1 & 0 & 0 \\ 0 & 0 & 0 & 0 & -a_{12} & a_{10} & -a_8 & a_6 & -a_4 & a_2 & -a_0 & 0 \\ 0 & 0 & 0 & 0 & 0 & -a_{11} & a_9 & -a_7 & a_5 & -a_3 & a_1 & 0 \\ 0 & 0 & 0 & 0 & 0 & a_{12} & -a_{10} & a_8 & -a_6 & a_4 & -a_2 & a_0 \end{bmatrix} \tag{A.2}$$

$$D_n = \begin{bmatrix} a_{11} & -a_9 & a_7 & -a_5 & a_3 & -a_1 & 0 & 0 & 0 & 0 & 0 & 0 \\ -a_{12} & a_{10} & -a_8 & a_6 & -a_4 & a_2 & -a_0 & 0 & 0 & 0 & 0 & 0 \\ 0 & -a_{11} & a_9 & -a_7 & a_5 & -a_3 & a_1 & 0 & 0 & 0 & 0 & 0 \\ 0 & a_{12} & -a_{10} & a_8 & -a_6 & a_4 & -a_2 & a_0 & 0 & 0 & 0 & 0 \\ 0 & 0 & a_{11} & -a_9 & a_7 & -a_5 & a_3 & -a_1 & 0 & 0 & 0 & 0 \\ 0 & 0 & -a_{12} & a_{10} & -a_8 & a_6 & -a_4 & a_2 & -a_0 & 0 & 0 & 0 \\ 0 & 0 & 0 & -a_{11} & a_9 & -a_7 & a_5 & -a_3 & a_1 & 0 & 0 & 0 \\ 0 & 0 & 0 & a_{12} & -a_{10} & a_8 & -a_6 & a_4 & -a_2 & a_0 & 0 & 0 \\ 0 & 0 & 0 & 0 & a_{11} & -a_9 & a_7 & -a_5 & a_3 & -a_1 & 0 & 0 \\ 0 & 0 & 0 & 0 & -a_{12} & a_{10} & -a_8 & a_6 & -a_4 & a_2 & -a_0 & 0 \\ 0 & 0 & 0 & 0 & 0 & -a_{11} & a_9 & -a_7 & a_5 & -a_3 & a_1 & 0 \\ 0 & 0 & 0 & 0 & 0 & a_{12} & -a_{10} & a_8 & -a_6 & a_4 & -a_2 & a_0 \end{bmatrix} \tag{A.3}$$